JOURNAL OF PROPULSION AND POWER
Vol. 16, No. 1, January–February 2000

Evaluation of Boundary Conditions for the Gust–Cascade Problem

R. Hixon,* S.-H. Shih,† and R. R. Mankbadi‡
NASA John H. Glenn Research Center at Lewis Field, Cleveland, Ohio 44135

Using a high-order-accuracy finite difference time-domain algorithm, the acoustic scattering from a flat-plate cascade is computed. Keeping the grid and time step fixed, the effect of four different boundary conditions on the accuracy, stability, and convergence of the computed solution is compared. Although none of the boundary conditions tested gave a perfect solution, the Giles and perfectly matched layer boundary conditions performed well.

Nomenclature

A	= gust amplitude
c_1, c_2, c_3, c_4	= one-dimensional characteristics
c_∞	= mean speed of sound
E	= total energy
f, g	= correction variables for Hagstrom boundary condition
p	= pressure
Q, P, Ψ	= damping variables in perfectly matched layer boundary condition
U_∞	= mean velocity
u, v	= velocities in the x and y directions
x, y	= grid coordinate directions
α	= gust wave number in the x direction
β	= gust wave number in the y direction
γ	= ratio of specific heats
Δt	= time step
$\Delta x, \Delta y$	= grid spacing in the x and y directions
ρ	= density
σ	= damping coefficient in perfectly matched layer boundary condition
ω	= gust frequency
$\prime$	= perturbation quantity
$\bar{}$	= mean quantity

Introduction

DESPITE recent efforts to introduce quieter aircraft, it is expected that noise will increase as a barrier to air transportation.[1–3] For high-bypass jet engines, fan noise becomes comparable to jet noise.[4] With current emphasis placed on jet noise reduction, fan noise could become the dominant noise source in the near future. Fan noise can be classified into three main sources[5]: inlet boundary layer or inflow distortions interacting with the fan, self noise from the fan, and fan wakes interacting with stators or struts. Both tone noise and broadband noise can be generated.

The gust–cascade interaction can be taken as representing the interaction of inflow disturbances with the fan or the interaction of the fan wakes the stator.[6,7] In the simplest gust–cascade model, the blades are represented as two-dimensional flat-plate cascades stacked in the spanwise direction. The inflow distortions or the fan wakes are represented by vortical gusts convected with the mean flow. The interaction of the gust with the blades produces unsteady pressure distribution over the blades' surfaces. If this unsteady surface pressure is coupled to the propagation duct modes inside the nacelle, the radiated inlet and exhaust sound can be obtained. Classical work on the gust–cascade problem has relied on approximate analysis and empirical formulation and is reviewed by Huff.[5] The two-dimensional gust–cascade interaction has been studied by Kaji and Okazaki.[8] Three-dimensional effects are considered by Namba,[9] who pointed out that three-dimensional effects become less important at high acoustic-response frequencies. Effects of loading and non-uniform transonic flow are given by Atassi et al.[10] Effects of camber, thickness, and stagger angles are given in Lorence and Hall.[11]

In the present decade, considerable progress in the relatively new science of computational aero-acoustics (CAA) has been achieved. In CAA, the unsteady governing equations are discretized and solved for time-dependent flow variables, which includes the mean flow and the flow or acoustic disturbances. High-order schemes are required for discretization to reduce dissipation and dispersion errors. But high-order schemes support the formation of spurious modes at the boundaries of the computational domain. Careful attention for unsteady boundary treatment is needed to produce the physically correct disturbance field.

Considerable progress has been made in applying CAA to jet noise (see review articles by Tam[12] and Mankbadi.[13] Application of CAA to fan noise is still limited and it is required to demonstrate first the ability of CAA to accurately predict simple models of fan-noise elements. To achieve this purpose, the gust–cascade model was considered as a benchmark problem in the second workshop on benchmark problems for CAA.[14] The amplitude of the gust was taken to be small; thus, either the linearized or the full Euler equations can be used and comparison with analytical theories can be made. The objective was to demonstrate what CAA algorithms can offer as eventual substitute for simpler source models. Several algorithms were used to compute this problem,[15–17] and the results were compared to a solution from Hall.[18] The computed results, however, varied considerably from Hall's solution and from each other.

It is suspected that the unsteady boundary treatment could be responsible for the discrepancy between the preceding simulations of the same gust–cascade problem. This might be particularly true for the time-domain simulations, where no exact boundary treatment exists. This issue is addressed in this paper. We show that the inflow and outflow treatment has considerable influence on the solution. Some boundary treatments are shown to produce satisfactory agreement with theory given a longer computational domain.

Problem Statement

This benchmark problem consists of four flat-plate airfoils in an unstaggered cascade, shown in Fig. 1. In this problem, a periodic

Presented as Paper 98-2489 at the AIAA 2nd Theoretical Fluid Mechanics Meeting, Albuquerque, NM, 15–18 June 1998; received 5 July 1998; revision received 14 December 1998; accepted for publication 16 December 1998. Copyright © 1999 by the American Institute of Aeronautics and Astronautics, Inc. No copyright is asserted in the United States under Title 17, U.S. Code. The U.S. Government has a royalty-free license to exercise all rights under the copyright claimed herein for Governmental purposes. All other rights are reserved by the copyright owner.

*Senior Research Associate, Institute for Computational Mechanics in Propulsion.
†Senior Research Associate, Institute for Computational Mechanics in Propulsion.
‡Technical Leader, Computational Aeroacoustics, Institute for Computational Mechanics in Propulsion.

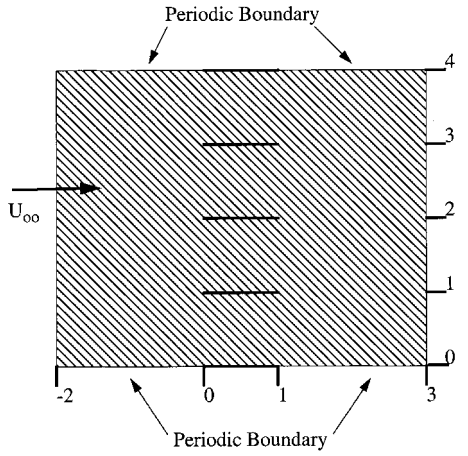

Fig. 1 Turbomachinery noise benchmark problem.

vortical gust is convected in a uniform mean flow, impinging on the flat-plate cascade and radiating noise upstream and downstream. At the inflow boundary, the mean flow and vortical gusts are defined as

$$U_{\infty}/c_{\infty} = 0.5, \qquad u_{\text{gust}} = (A\beta/\alpha)\cos(\alpha x + \beta y - \omega t)$$
$$v_{\text{gust}} = A\cos(\alpha x + \beta y - \omega t) \tag{1}$$

where

$$A = 0.01, \qquad \alpha = \beta = \omega = 5\pi/2 \tag{2}$$

The computational domain is limited to

$$-2 \le x \le 3, \qquad 0 \le y \le 4 \tag{3}$$

This problem is to be solved with either the linearized or the full Euler equations. The output requested is 1) the real imaginary component of the pressure jump across the airfoil, and 2) the intensity of the radiated sound $\bar{P}^2$ at the inflow and outflow boundaries.

Governing Equations and Numerical Formulation

The conservative two-dimensional Euler equations in Cartesian coordinates are given as:

$$\begin{Bmatrix} \rho \\ \rho u \\ \rho v \\ E \end{Bmatrix}_t + \begin{Bmatrix} \rho u \\ \rho u^2 + p \\ \rho uv \\ n(E+p) \end{Bmatrix}_x + \begin{Bmatrix} \rho v \\ \rho uv \\ \rho v^2 + p \\ v(E+p) \end{Bmatrix}_y = 0 \tag{4}$$

where

$$p = (\gamma - 1)\left[E - \tfrac{1}{2}\rho(u^2 + v^2)\right] \tag{5}$$

The numerical solver is a high-order accurate finite difference time-domain scheme. The spatial derivatives are computed using a prefactored sixth-order compact scheme[19] utilizing an explicit tenth-order filter,[20] and the time integration is performed using Hu et al.'s[21] 5-6 low dispersion and dissipation Runge–Kutta method. The grid used is a uniform Cartesian grid where $\Delta x = \Delta y = 0.02$. Because the vortical gust has a wavelength of 0.8, this gives 40 points per wavelength, which produces a linear dispersion error of 1.e-9.

For all calculations, the time step used was $\Delta t = 0.0125$, which corresponds to a Courant–Friedrichs–Lewy number of 1.2.

Boundary Condition Formulation

Thompson Boundary Condition

The Thompson boundary condition[22,23] uses a one-dimensional characteristic theory to determine the proper boundary-condition specification. In the Thompson method, the boundary condition is only applied to the derivatives normal to the boundary; the tangential derivative terms are considered to be a source term. Thus, Eq. (4) becomes

$$\begin{Bmatrix} \rho \\ \rho u \\ \rho v \\ E \end{Bmatrix}_t + \begin{Bmatrix} \rho u \\ \rho u^2 + p \\ \rho uv \\ u(E+p) \end{Bmatrix}_x = \{S\} \tag{6}$$

The normal flux derivative term is then linearized and decomposed into one-dimensional characteristics:

$$(c_1)_t + (\bar{u} - \bar{c})(p'_x - \bar{\rho}\bar{c}u'_x) = 0, \qquad (c_2)_t + \bar{u}(\bar{c}^2\rho'_x - p'_x) = 0$$
$$(c_3)_t + \bar{u}v'_x = 0, \qquad (c_4)_t + (\bar{u} + \bar{c})(p'_x + \bar{\rho}\bar{c}u'_x) = 0 \tag{7}$$

Thus, at the outflow boundary

$$\rho' = \rho - \bar{\rho}, \qquad u' = u - \bar{u}$$
$$v' = v - \bar{v}, \qquad p' = p - \bar{p} \tag{8}$$

However, the incoming vortical gust must be specified at the inflow boundary. To accomplish this

$$\rho' = \rho - \bar{\rho}, \qquad u' = u - \bar{u} - u_{\text{gust}}$$
$$v' = v - \bar{v} - v_{\text{gust}}, \qquad p' = p - \bar{p} \tag{9}$$

The characteristics given in Eq. (7) represent, respectively, the left-running acoustic wave, the entropy wave, the vorticity wave, and the right-running acoustic wave. In Thompson's approach, the direction of travel of the characteristic determines if it is propagating into or out of the domain. The characteristics that are propagating out of the domain are left unchanged; those propagating into the domain are set to zero.

Once the characteristics are determined, the time derivatives of the primitive variables are given as

$$\rho_t = \frac{[2(c_2)_t + (c_1)_t + (c_4)_t]}{2\bar{c}^2}, \qquad p_t = \frac{(c_1)_t + (c_4)_t}{2}$$
$$u_t = \frac{(c_4)_t - (c_1)_t}{2\bar{\rho}\bar{c}}, \qquad v_t = (c_3)_t \tag{10}$$

With the primitive variables now known, the time derivative of the conserved variables are calculated as

$$(\rho u)_t = \bar{\rho}u_t + \bar{u}\rho_t, \qquad (\rho v)_t = \bar{\rho}v_t$$
$$E_t = \tfrac{1}{2}(\bar{u}^2)\rho_t + [p_t/(\gamma - 1)] + \bar{\rho}\bar{u}u_t \tag{11}$$

Giles Boundary Condition

The Giles boundary condition[24] resembles the Thompson boundary condition in that they are both based on one-dimensional characteristics. However, instead of decomposing the equations into normal and tangential components, Giles considered only the normal component and formulated corrections for the effect of the tangential component. Thus, while Thompson's analysis was geared toward only normal and tangential one-dimensional waves, Giles' analysis allows for waves with other angles of incidence.

To apply the Giles boundary condition, the interior equations are used at the boundary to compute the time derivatives. The one-dimensional characteristics are then defined as

$$(c_1)_t = p'_t - \bar{\rho}\bar{c}u'_t, \qquad (c_2)_t = \bar{c}^2\rho'_t - p'_t$$
$$(c_3)_t = \bar{\rho}\bar{c}v'_t, \qquad (c_4)_t = p'_t + \bar{\rho}\bar{c}u'_t \tag{12}$$

The outgoing characteristics are left unchanged, but the incoming characteristics are modified to account for the angle of incidence of the outgoing wave. At the inflow boundary

$$(c_2)_y = \bar{c}^2\rho'_y - \rho'_y, \qquad (c_3)_y = \bar{\rho}\bar{c}v'_y, \qquad (c_4)_y = p'_y + \bar{\rho}\bar{c}u'_y \tag{13}$$

The time derivatives of the characteristics are computed using

$$(c_2)_t + \bar{v}(c_2)_y = 0$$

$$(c_3)_t + \bar{v}(c_3)_y + \tfrac{1}{2}[(\bar{u} + \bar{c})(c_4)_y + (\bar{u} - \bar{c})(c_1)_y] = 0$$

$$(c_4)_t + (\bar{v})(c_4)_y - \tfrac{1}{2}[(\bar{u} - \bar{c})(c_3)_y] = 0 \tag{14}$$

To account for the incoming vortical gust, the variables are decomposed as shown in Eq. (9). Once the time derivatives of the characteristics are known, Eqs. (10) and (11) are used to determine the time derivatives of the conserved variables.

At the outflow boundary, only one characteristic is corrected. The variables are decomposed as shown in Eq. (8), and the tangential derivatives are taken:

$$(c_1)_y = p'_y - \bar{\rho}\bar{c}u'_y, \qquad (c_3)_y = \bar{\rho}\bar{c}v'_y \tag{15}$$

The incoming characteristic is updated as

$$(c_1)_t + \bar{u}(c_3)_y + \bar{v}(c_1)_y = 0 \tag{16}$$

Hagstrom Boundary Condition

Again, like the Giles equations, the Hagstrom boundary condition[25] is formulated in terms of the one-dimensional normal characteristics:

$$(c_1) = p' - \bar{\rho}\bar{c}u', \qquad (c_2) = \bar{c}^2\rho - p'$$

$$(c_3) = \bar{\rho}\bar{c}v', \qquad (c_4) = p' + \bar{\rho}\bar{c}u' \tag{17}$$

As in the Giles boundary condition, the incoming characteristics are corrected while the outgoing characteristics are left unchanged. However, unlike the Giles boundary condition, the corrections are determined by solving additional equations at the boundary, with the user determining how many equations are needed for accuracy. The effect of these equations is to match to increasing order the short time expansion of the exact boundary solution.

The inflow boundary condition takes the following form:

$$(c_2)_t = 0, \qquad (c_3)_t + \bar{\rho}\bar{c}\left(\bar{u}u'_y + \bar{v}v'_y + \frac{1}{\bar{\rho}}p'_y\right) = 0$$

$$(c_4)_t + \bar{v}(c_4)_y + \frac{1}{2}\bar{\rho}\bar{c}(\bar{c} - \bar{u})v'_y + \frac{1}{2}\sum_{j=1}^{N}(f_j + g_j) = 0 \tag{18}$$

Here, f and g are the correction equations, which are given by

$$(f_j)_t + (\bar{v} + C)(f_j)_y + S(c_4)_{yy} = 0$$

$$(g_j)_t + (\bar{v} - C)(g_j)_y + S(c_4)_{yy} = 0 \tag{19}$$

where

$$C = \sqrt{\bar{c}^2 - \bar{u}^2}\cos\left(\frac{j\pi}{2N+1}\right)$$

$$S = \frac{(\bar{c}^2 - \bar{u}^2)}{2N+1}\left[\sin\left(\frac{j\pi}{2N+1}\right)\right]^2 \tag{20}$$

For the inflow condition, the prime terms are defined in Eq. (9). The outflow condition is written as

$$(c_1)_t + \bar{v}(c_1)_y + \bar{\rho}\bar{c}\bar{u}v'_y + \sum_{j=1}^{N}(f_j + g_j) = 0 \tag{21}$$

Here, the correction equations are given by

$$(f_j)_t + (\bar{v} + C)(f_j)_y + S(p')_{yy} = 0$$

$$(g_j)_t + (\bar{v} - C)(g_j)_y + S(p')_{yy} = 0 \tag{22}$$

For the outflow equations, the prime terms are defined in Eq. (8).

Perfectly Matched Layer

In the perfectly matched layer (PML) boundary condition, a numerical sponge layer is constructed that surrounds the domain of interest. When a wave propagates into this layer, it is damped with little or no reflection, regardless of the angle of incidence or the wavelength of the incident wave.

The PML used here is that of Abarbanel et al.[26] In their approach, the Euler equations are linearized about a uniform mean flow in the x direction. A transformation is applied to the equations, and a PML layer is constructed mathematically. For the cascade problem, the sponge layer is only in the x direction; however, the original derivation includes the y direction terms as well. The reduced PML equations are given as

$$u'_t + Mu'_x + p'_x = -\sigma(u' + Mp')$$

$$v'_t + Mv'_x + p'_y = -\sigma(v' + 2Q + \sigma\Psi) + \sigma_x MP$$

$$p'_t + Mp'_x + u'_x + v'_y = -\sigma(Mu' + p')$$

$$Q_t + (1 - M^2)p'_y = 0$$

$$P_t = (1 - M^2)(v' - \sigma P), \qquad \Psi_t = (1 - M^2)Q \tag{23}$$

Here, the σ denotes the damping factor, which varies through the layer as

$$\sigma(x) = 40\left(\frac{x - x_{\text{start}}}{x_{\text{end}} - x_{\text{start}}}\right)^2 \tag{24}$$

To implement these equations into the nonlinear code, the equations are transformed into

$$(u'_t)_{\text{PML}} = -\sigma(u' + Mp')$$

$$(v'_t)_{\text{PML}} = -\sigma(v' + 2Q + \sigma\Psi) + \sigma_x MP$$

$$(p'_t)_{\text{PML}} = -\sigma(Mu' + p'), \qquad Q_t + (1 - M^2)p'_y = 0$$

$$P_t = (1 - M^2)(v' - \sigma P), \qquad \Psi_t = (1 - M^2)Q \tag{25}$$

As before, the prime quantities are determined using Eq. (8) at the outflow, and Eq. (9) at the inflow. This formulation does not include the density equation; to complete the equation set, the flow is assumed to be isentropic:

$$\bar{c}^2(\rho'_t)_{\text{PML}} = (p'_t)_{\text{PML}} \tag{26}$$

Once the PML corrections are calculated, they are converted into conserved variables using Eq. (11) and added to the time derivatives computed using the nonlinear Euler equations.

In all calculations, a 20-point PML layer was employed.

Wall Boundary Condition

On the flat plates, the wall condition of Tam and Dong[27] was used. In this method, the time derivative of the velocity normal to the wall is set to zero:

$$(\rho v)_t = 0 \tag{27}$$

To accomplish this, the time derivative of the normal velocity at the wall is expanded:

$$(\rho uv)_x + (\rho v^2 + p)_y = v[(\rho u)_x + (\rho v)_y]$$

$$+ (\rho u)v_x + (\rho v)v_y + p_y = p_y = 0 \tag{28}$$

To set the normal pressure derivative to zero, a ghost point was used inside the wall for only the normal pressure derivative. All other derivatives are taken with fully one-sided differences.

At the leading and trailing edges of the plates, the wall condition is set on both the upper and lower surfaces. To make these points single-valued, the result is then averaged and used on the upper and lower surfaces.

Numerical Results

Two tests were performed for each boundary condition. In both tests, the mean flow was initialized as

$$\bar{\rho} = 1, \qquad \bar{u} = 0.5, \qquad \bar{v} = 0, \qquad \bar{p} = 1/\gamma \tag{29}$$

The perturbations were initialized as

$$\rho_{\text{gust}}(x, y, 0) = 0$$

$$u_{\text{gust}}(x, y, 0) = -q(x)(A\beta/\alpha)\cos(\alpha x + \beta y - \omega t)$$

$$v_{\text{gust}}(x, y, 0) = -q(x)A\cos(\alpha x + \beta y - \omega t)$$

$$p_{\text{gust}}(x, y, 0) = 0 \tag{30}$$

where

$$q(x) = \begin{cases} 1 & x < -2 \\ \frac{1}{2} + \frac{1}{2}\cos[(\pi/2)(x+2)] & -2 < x < 0 \\ 0 & x > 0 \end{cases} \tag{31}$$

In the first test, the cascade is removed from the domain, and the ability of the boundary condition to allow the flow to reach a periodic state is tested. In the second test, the cascade is placed in the flow and the result is compared with the semianalytic result.

Test Problem 1: No Cascade

In the first test problem, the domain was initialized with the perturbation given in Eq. (30), and the cascade was removed. This tests the implementation of the upstream disturbance as well as the ability of the outflow boundary condition to allow the vortical gust to convect out without reflection. The grid for all cases had a uniform spacing of $\Delta x = \Delta y = 0.02$.

In these problems, the time history of pressure is shown at two points, $(-2, 0)$ and $(3, 0)$. Figures 2 and 3 show the pressure time history at these two points for the different boundary conditions. From top to bottom, the graphs show the Thompson boundary condition, the Giles, the Hagstrom boundary condition, using 3 equations, the Hagstrom boundary condition using 10 equations, and the PML boundary condition. Notice that the scales are all similar except for the Thompson boundary condition, which does not give an adequate solution for this problem. Also, the 10-equation Hagstrom condition does not give a better solution than the 3-equation Hagstrom boundary condition. This is not surprising, as the Hagstrom BC is designed to perform well for transients and not for long-term time marching, and, as the number of auxiliary equations is increased, the long-time solution may be less accurate.

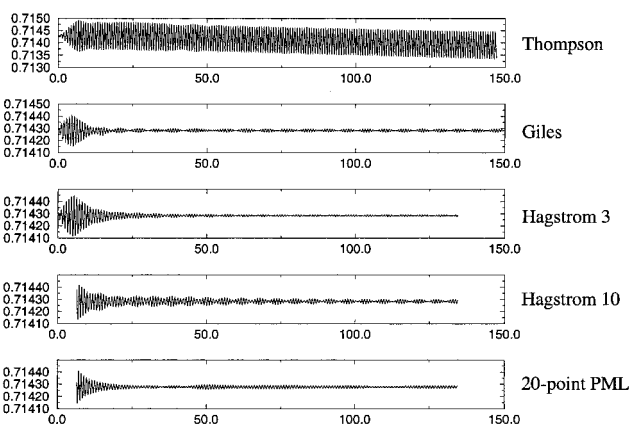

Fig. 2 Pressure time history at inflow boundary point (− 2, 0).

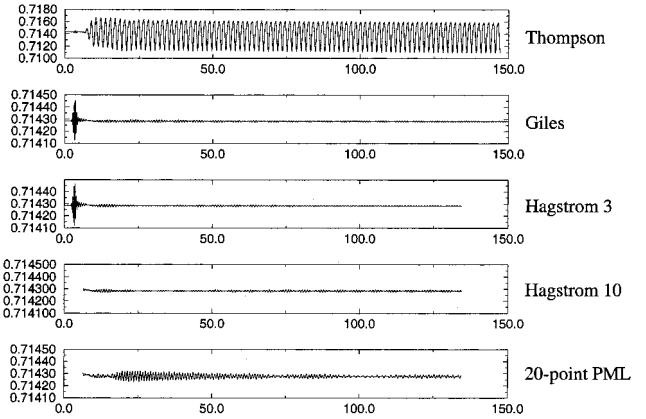

Fig. 3 Pressure time history at outflow boundary point (3, 0).

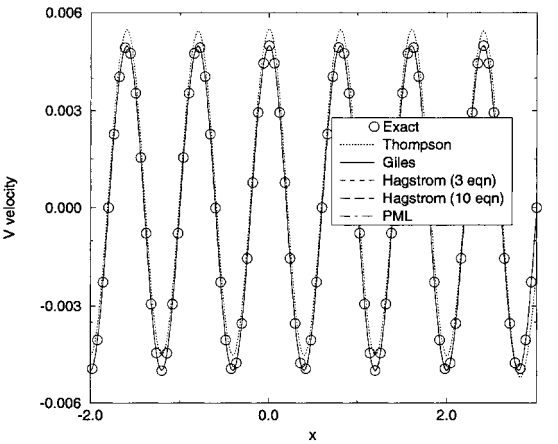

Fig. 4 v velocity distribution along $y = 0$ line.

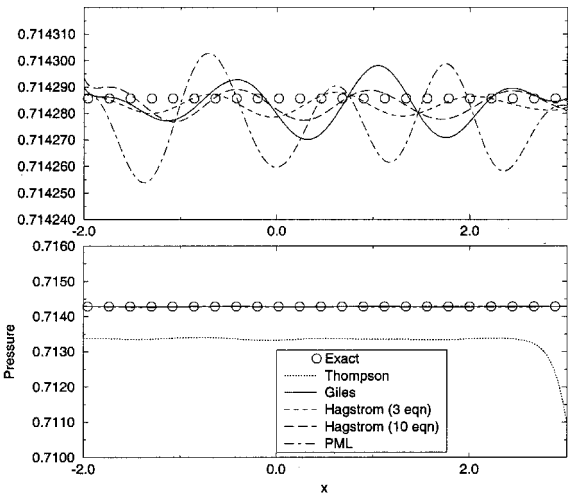

Fig. 5 Pressure distribution along $y = 0$ line.

Figures 4 and 5 show the v velocity and pressure distributions along the $y = 0$ line. The inflow vorticity specification is working well, as shown in Fig. 4. Figure 5 illustrates the pressure error, which is mainly due to the boundary conditions reflecting the outgoing vorticity and the acoustic waves generated by the initial vorticity specification. From Fig. 5, the Thompson condition is giving a much worse solution than the other boundary conditions; the other boundary conditions have roughly equivalent levels of error.

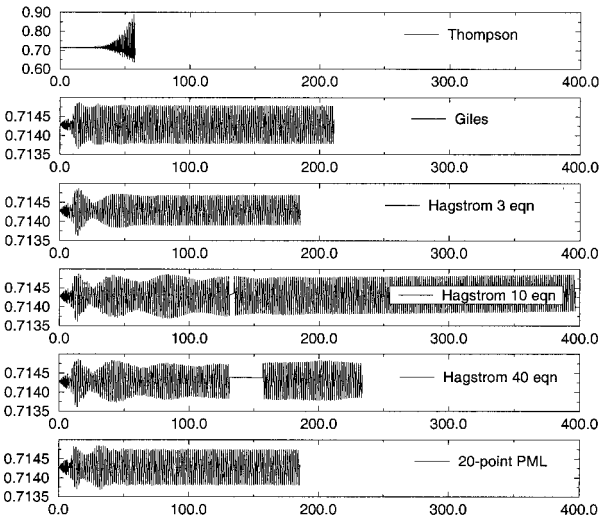

Fig. 6 Pressure time history at inflow boundary point (− 2, 0).

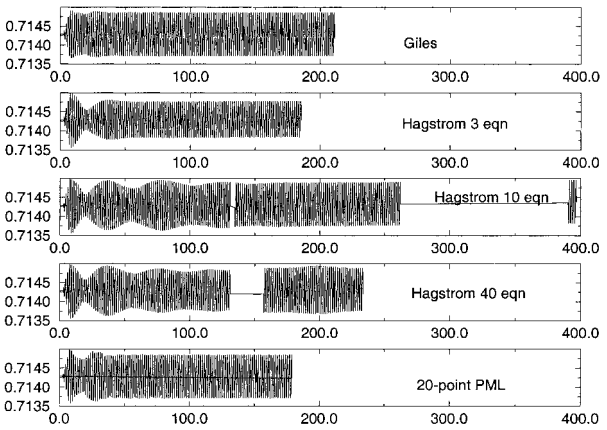

Fig. 7 Pressure time history at outflow boundary point (3, 0).

Test Problem 2: Specified Domain Calculation

The next calculations were performed on the specified domain, which covered $-2 < x < 3$. All of the boundary conditions were tested for this configuration.

Figures 6 and 7 show the pressure time history at the inflow and outflow boundary points. Some of the data are fragmentary; this is due to accidental deletions and should be disregarded.

The Thompson boundary condition proved to be unstable due to reflections from the inflow boundary interacting with the cascade and initiating a nonphysical feedback loop. Figure 6 illustrates the rapid buildup of pressure in the domain.

The Hagstrom boundary conditions were very slowly unstable for this problem, as the very slow increase in mean pressure in Figs. 6 and 7 show. As expected, adding more equations at the boundary improved the transient solution; however, the long-time periodic solution was not improved. Also, as more equations were added, the solutions took longer to converge. Again, it must be noted that the Hagstrom boundary condition was developed for transient problems and not for long-time periodic problems.

Both the Giles and the PML boundary conditions allowed a stable long-term solution to be calculated. The PML condition required extra points in the buffer zone; however, it did somewhat improve the solution at the boundary.

Figures 8 and 9 show the rms pressure results calculated using these boundary conditions. All solutions were in the same range, with the PML boundary condition performing slightly better than the rest.

Figure 10 shows the pressure difference across the $y = 0$ airfoil for the Giles boundary condition; all of the stable boundary conditions allowed identical airfoil results to be obtained. The effect of the numerical singularities at the leading and trailing edge are illustrated. Wall conditions were applied for the upper and lower leading- and trailing-edge points, with the results being averaged and applied to both points.

It must be noted that these singularities are purely due to the infinitely thin airfoils prescribed in the problem statement; it is expected that these singularities are the main factor causing the error on the airfoil. Future work will address the effects of real airfoil geometries.

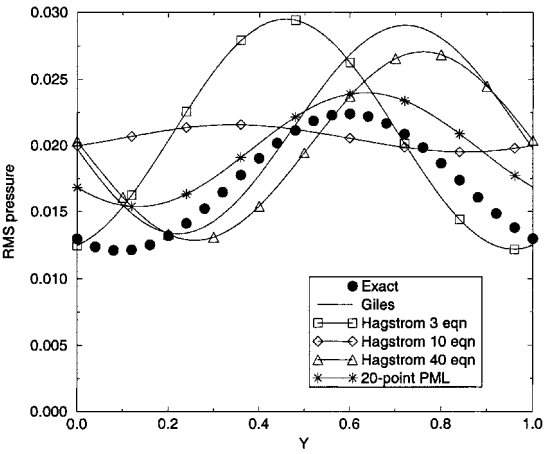

Fig. 8 Root-mean-square pressure at upstream boundary ($x = -2$).

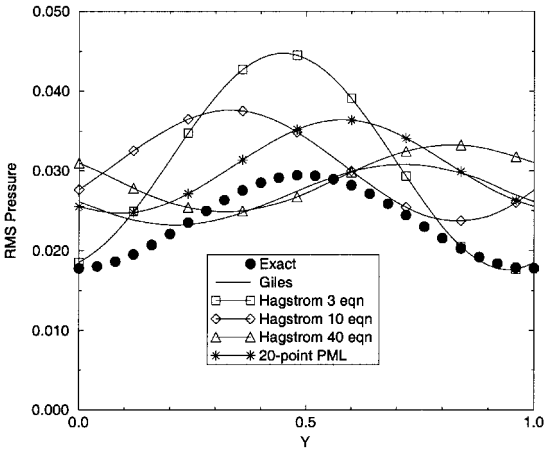

Fig. 9 Root-mean-square pressure at downstream boundary ($x = 3$).

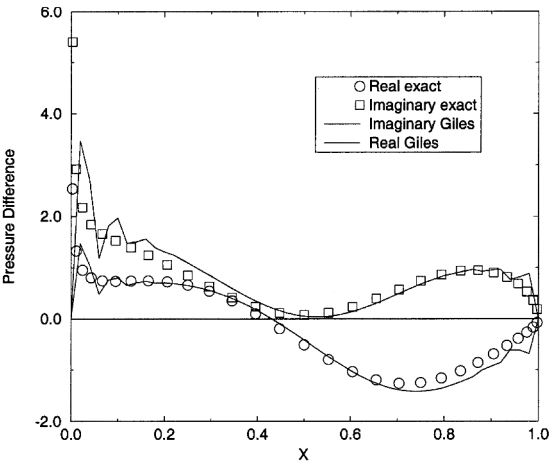

Fig. 10 Comparison of airfoil pressure distribution with exact solution.

Test Problem 3: Long Domain Calculation

To quantify the relative effect of the numerical singularities and the close boundaries on the computed solution, the same calculation was performed on a long domain ($-8 < x < 9$) using the same grid spacing and time step. For these calculations, which required much more CPU time to converge, only the Giles and PML boundary conditions were used. Figure 11 shows that the solution on the airfoil does not change as compared to the short domain solution.

Figures 12 and 13 show the computed rms pressure disturbances at the upstream and downstream locations. Using this long domain,

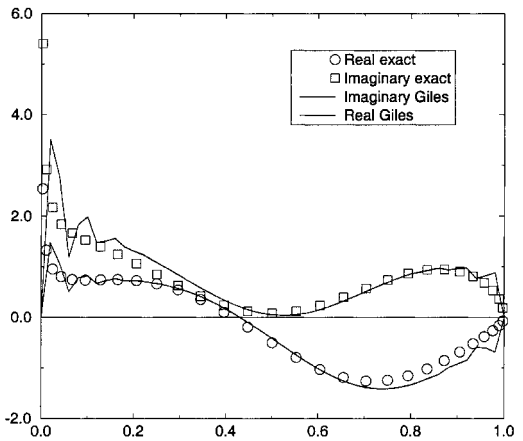

Fig. 11 Comparison of airfoil pressure distribution for longdomain solution.

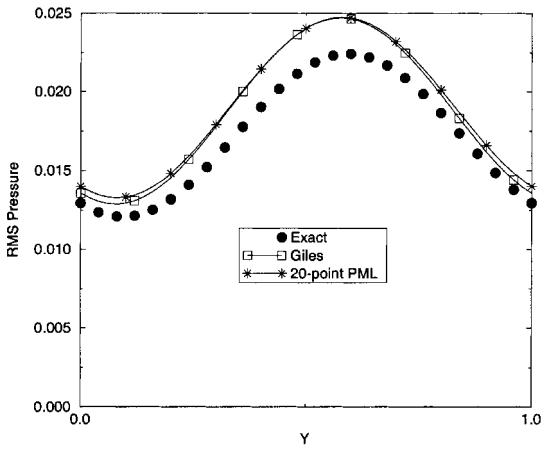

Fig. 12 Upstream rms pressure distribution for long-domain calculation ($x = -2$).

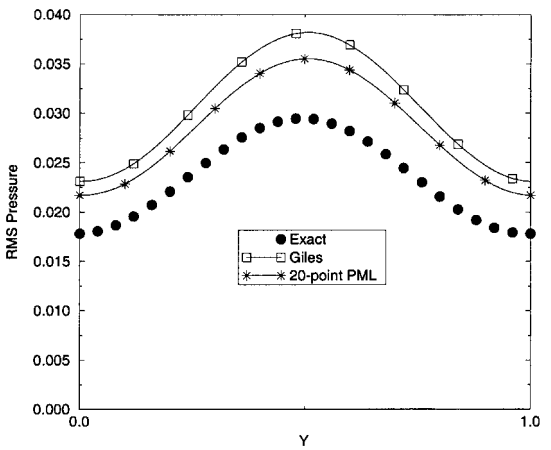

Fig. 13 Downstream rms pressure distribution for long-domain calculation ($x = 3$).

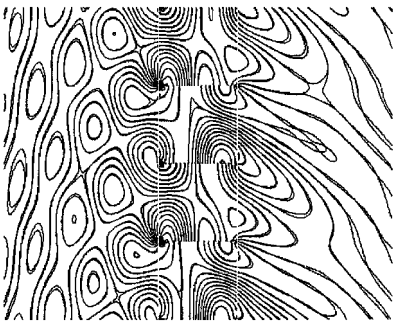

Fig. 14 Comparison of specified-domain and long-domain instantaneous pressure contours with Giles boundary conditions.

both boundary conditions give a solution that is close to the exact solution in phase, with a greater amplitude. It is theorized that the errors in the pressure on the airfoil due to the numerical singularities are causing the amplitude error. However, the PML outflow condition is performing better than the Giles outflow condition, as shown in Fig. 13.

Figure 14 shows the effect of the extended domain on the pressure contours using the Giles boundary condition. On the airfoil itself, the contours are nearly identical. In the upstream direction, the contours become different as the inflow boundary is approached, showing that there is some reflection from the inflow boundary condition. In the downstream direction, however, the contours diverge almost immediately after the trailing edge, suggesting that the outflow boundary condition is more reflective than the inflow.

Conclusions

Several boundary conditions were tested on a CAA workshop benchmark cascade problem. The problem is very difficult due to numerical singularities in the problem specification as well as the proximity of the boundaries. Because the problem is periodic in one direction, the ability of the boundary condition to allow acoustic and vortical waves to exit without reflection determines the stability and accuracy of the solution. It was found that the error due to the numerical singularities at the leading and trailing edges of the flat plates kept the solver from obtaining the exact amplitude of the radiated sound; however, the reflected waves at the boundaries due to the boundary conditions kept the solver from obtaining the correct radiation pattern, even though the airfoil pressure distribution was nearly identical.

Of the four boundary conditions tested, the Thompson condition was found to have the highest reflection at the boundaries, resulting in code instability. The Giles condition did reasonably well while requiring very little extra computational work. The Hagstrom condition did not perform well for this problem, but it must be noted that it is designed for short-term transient calculations and not long-term periodic problems such as this one. The PML boundary condition performed the best, but required a 20-point sponge layer at each end. However, the performance of the PML condition could most likely be improved with better specification of the damping coefficient distribution in the sponge layer.

It must be noted, however, that all of these boundary conditions are linearized about the mean flow, and three of the four are linearized about a uniform mean flow. Because this test problem had an identifiable uniform mean flow, this was a best case test for these boundary conditions. It is not certain what effect nonuniform mean flows and nonperiodic domains would have on the accuracy of these boundary conditions.

Currently, boundary condition specification is one of the main sources of error in time-domain CAA calculations. Work in this area will yield large dividends.

Acknowledgments

This work was carried out under Grant NCC3-531 from the NASA Lewis Research Center. L. A. Povinelli was the Technical Monitor.

References

[1]Russo, C. J., "Changing the Landscape of Civil Aviation," *13th International Symposium on Air Breathing Engines*, ISABE Paper 97-7002, Chattanooga, TN, Sept. 1997.

[2]Batterton, P., "Civil Transport Aircraft Propulsion Challenges and NASA Advanced Subsonic Technology Program," *13th International Symposium on Air Breathing Engines*, ISABE Paper 97-7044, Chattanooga, TN, Sept. 1997.

[3]Shaw, R. J., "Progress Toward Meeting the Propulsion Technology Challenges for a 21st Century High Speed Civil Transport," *13th International Symposium on Air Breathing Engines*, ISABE Paper 97-7045, Chattanooga, TN, Sept. 1997.

[4]Groenewig, J. F., Sofrin, T. G., and Rice, E. J., and Gliebe, P. R., "Aeroacoustics of Flight Vehicles: Theory and Practice," *Turbomachinery Noise*, edited by H. Hubbard, NASA PRE-1258, Vol. 1, Aug. 1991, pp. 151–209.

[5]Huff, D. L., "Fan Noise Prediction: Status and Needs," NASA/TM-97206533, Dec. 1998; also AIAA Paper 98-0177, Jan. 1998.

[6]Ventres, C. S., Thebald, M. A., and Mark, W. D., "Turbofan Noise Generation," NASA CR-167952, Vols. 1 and 2, 1982.

[7]Meyer, H. D., and Envia, E., "Aeroacoustic Analysis of Turbofan Noise Generation," NASA CR-4715, March 1996.

[8]Kaji, S., and Okazaki, T., "Generation of Sound by Rotor-Stator Interaction," *Journal of Sound and Vibration*, Vol. 13, No. 3, 1970, pp. 281–307.

[9]Namba, M., "Three-Dimensional Analysis of Blade Force and Sound Generation for an Annular Cascade in Distorted Flows," *Journal of Sound and Vibration*, Vol. 50, No. 4, 1977, pp. 479–508.

[10]Atassi, H., Fang, J., and Hardy, B., "Sound Radiated from a Loaded Cascade in Nonuniform Transonic Flow," AIAA Paper 96-1756, May 1996.

[11]Lorence, C. B., and Hall, K. C., "Sensitivity Analysis of the Aeroacoustic Response of Turbomachinery Blade Rows," AIAA Paper 95-0166, Jan. 1995.

[12]Tam, C. K. W., "Computational Aeroacoustics: Issues and Methods," AIAA Paper 95-0677, Jan. 1995.

[13]Mankbadi, R. R., "Computational Aero-Acoustics in Propulsion System," *Journal of Propulsion and Power*, Vol. 15, No. 4, 1999, pp. 504–512.

[14]Tam, C. K. W., and Hardin, J. C., *2nd Computational Aeroacoustics Workshop on Benchmark Problems*, edited by C. K. W. Tam and J. Hardin, NASA CP-3352, June 1997, pp. 1–8.

[15]Hu, F. Q., and Manthey, J. L., "Application of PML Absorbing Boundary Conditions to the Benchmark Problems in Computational Aeroacoustics," *2nd Computational Aeroacoustics Workshop on Benchmark Problems*, edited by C. K. W. Tam and J. Hardin, NASA CP-3352, 1997, pp. 119–152.

[16]Lockard, D. A., and Morris, P. J., "A Parallel Simulation of Gust/Cascade Interaction Noise," *2nd Computational Aeroacoustics Workshop on Benchmark Problems*, edited by C. K. W. Tam and J. Hardin, NASA CP-3352, 1997, pp. 279–288.

[17]Tam, C. K. W., Kurbatskii, K. A., and Fang, J., "Numerical Boundary Conditions for Computational Aeroacoustics Benchmark Problems," *2nd Computational Aeroacoustics Workshop on Benchmark Problems*, edited by C. K. W. Tam and J. Hardin, NASA CP-3352, 1997, pp. 191–220.

[18]Hall, K. C., "Exact Solution to Category 3 Problems—Turbomachinery Noise," *2nd Computational Aeroacoustics Workshop on Benchmark Problems*, edited by C. K. W. Tam and J. Hardin, NASA CP-3352, June 1997, pp. 41–43.

[19]Hixon, R., "A New Class of Compact Schemes," AIAA Paper 98-0367, Jan. 1998.

[20]Kennedy, C. A., and Carpenter, M. H., "Several New Numerical Methods for Compressible Shear-Layer Simulations," *Applied Numerical Mathematics*, Vol. 14, 1994, pp. 397–433.

[21]Hu, F. Q., Hussaini, M. Y., and Manthey, J. L., "Low-Dissipation and Low-Dispersion Runge-Kutta Schemes for Computational Acoustics," *Journal of Computational Physics*, Vol. 124, No. 1, 1996, pp. 177–191.

[22]Thompson, K. W., "Time-Dependent Boundary Conditions for Hyperbolic Systems," *Journal of Computational Physics*, Vol. 68, No. 1, 1987, pp. 1–24.

[23]Thompson, K. W., "Time-Dependent Boundary Conditions for Hyperbolic Systems, II," *Journal of Computational Physics*, Vol. 89, No. 2, 1990, pp. 439–461.

[24]Giles, M., "Nonreflecting Boundary Conditions for Euler Equation Calculations," *AIAA Journal*, Vol. 28, No. 12, 1990, pp. 2050–2058.

[25]Hagstrom, T., "On High-Order Radiation Boundary Conditions," *IMA Volume on Computational Wave Propagation*, edited by B. Engquist and G. Kriegsmann, Springer–Verlag, New York/Berlin, 1996, pp. 1–22.

[26]Abarbanel, S., Gottlieb, D., and Hesthaven, J., "Well-Posed Perfectly Matched Layer for Advective Acoustics," *Journal of Computational Physics*, Vol. 154, No. 2, 1999, pp. 266–293.

[27]Tam, C. K. W., and Dong, T. Z., "Wall Boundary Conditions for High-Order Finite-Difference Schemes in Computational Aeroacoustics," *Theoretical Computational Fluid Dynamics*, Vol. 6, No. 5–6, 1994, pp. 303–322.